Waste Management 211 (2026) 115308

Contents lists available at ScienceDirect

Waste Management

journal homepage: www.elsevier.com/locate/wasman

Research Paper

Assessing upcycling of waste bioplastics for production of sustainable carbon black substitute

Lukasz Niedzwiecki [a,*], Luca Fambri [b], Filippo Marchelli [a,c], Anna Pajdak [d], Marco Calvi [e], Luca Fiori [a,f]

[a] University of Trento, Department of Civil, Environmental and Mechanical Engineering, Via Mesiano 77, 38123 Trento, Italy
[b] Department of Industrial Engineering and INSTM Research Unit, University of Trento, Via Sommarive 9, 38123 Trento, Italy
[c] Department of Civil, Chemical and Environmental Engineering, University of Genova, Via all'Opera Pia 15a, 16145 Genova, Italy
[d] Strata Mechanics Research Institute of the Polish Academy of Sciences, Kraków, Poland
[e] Certottica S.c.r.l., Italian Institute of Certification of Optical Products Villanova Industrial Area, 32013 Longarone, Italy
[f] Center Agriculture Food Environment (C3A), University of Trento, San Michele all'Adige, Italy

ARTICLE INFO

Keywords:
Carbon black
Bioplastics
Waste
Upcycling
HTC
Pyrolysis

ABSTRACT

Carbon black is a product with multiple applications, including use as an additive for tyres or plastics, as well as ink or toner. Current methods of carbon black production are based on incomplete combustion of fossil fuels, followed by quenching, resulting in a high carbon footprint and related emissions. Even though unintended, biodegradable bioplastics at the end of life still pose problems to waste management plants. Most notably, the time required for bioplastics to biodegrade is longer than the typical residence time in state-of-the-art processes, such as anaerobic digestion and composting. This causes incomplete degradation and reduces the efficiency of waste treatment facilities. This work provides an experimental evaluation of a novel method of production of carbon black, using bioplastic waste (namely, cellulose acetate) as a feedstock. The proposed system consists of hydrothermal carbonisation (HTC) and subsequent pyrolysis of separated solid products. The novel product exhibits morphology and structure similar to commercial carbon black and high thermal stability. BET surface area as high as 175 m^2/g can be achieved by combining hydrothermal carbonisation performed at 250 °C followed by pyrolysis at 600 °C. Further increase in pyrolysis temperature provided no additional benefits and resulted in collapse of the pores within the mesoporous range, with detrimental influence on BET surface and pore volume.

1. Introduction

Carbon black is a material with a multitude of different applications, including use as a pigment (Pfaff, 2022), as an additive for the production of composites (Musenich et al., 2024), or coatings (Cheshmak et al., 2025), as well as a reinforcing filler in different types of products (Cataldi et al., 2016), including tyres (Pfaff, 2022) or mulching films (Hernandez-Charpak et al., 2024). Worldwide production of carbon black is nowadays close to 15 million tonnes/year, which is estimated to result in CO_2 emissions ranging between 29 and 79 million tonnes/year (Rosner et al., 2024). Generally, state-of-the-art carbon black production processes are based on the production of soot through incomplete combustion, followed by rapid quenching of the flue gases (Pfaff, 2022; Rosner et al., 2024). Feedstocks for the production of carbon black are usually fossil-based, including tar oils, petrochemical oils, or methane (Rosner et al., 2024). Recently, a lot of interest has been dedicated to plasma pyrolysis of methane, since such a method can produce hydrogen and carbon black, without significant CO_2 emissions if electricity from renewable sources is used (Mizeraczyk and Jasiński, 2016; Wen et al., 2025; Wnukowski, 2023). However, such an approach does not account for upstream emissions from the extraction of fossil natural gas, which could heavily impact the overall environmental performance of the subsequent use of such technology (Howarth, 2021; Howarth and Jacobson, 2021). One strategy for improving the environmental footprint of the production of carbon black is the pyrolysis of waste tyres (Aylón et al., 2008; Jiang et al., 2024, Jiang et al., 2023). However, this method essentially recovers carbon black from waste products of fossil-fuel origin. Recently, the use of biomass pyrolysis oil instead of fossil-

* Corresponding author.
E-mail address: lukasz.niedzwiecki@unitn.it (L. Niedzwiecki).

https://doi.org/10.1016/j.wasman.2025.115308
Received 21 July 2025; Received in revised form 24 November 2025; Accepted 20 December 2025
Available online 24 December 2025
0956-053X/© 2025 The Author(s). Published by Elsevier Ltd. This is an open access article under the CC BY license (http://creativecommons.org/licenses/by/4.0/).

based feedstocks has been proposed (Toth et al., 2018). Nonetheless, the environmentally friendly production of carbon black still requires significant efforts from the scientific community around the world.

Nowadays, increased attention is directed towards environmentally friendly management and processing of waste, with special focus on its use as a feedstock for clean production of different products (Čespiva et al., 2023; Jadlovec et al., 2024). Bioplastics are increasingly common in a multitude of different applications, due to the fact that they can be produced in a sustainable manner (Rosenboom et al., 2022) without the need for fossil sources. Despite improved biodegradability of bioplastics, when compared to fossil-based counterparts (Fambri et al., 2020), their processing still poses problems in modern waste management systems (Marchelli and Fiori, 2025). Thus, novel methods of processing these types of waste become increasingly attractive and necessary. Among bioplastics, cellulose acetate plays an important role, being used in many applications, including eyewear and safety glasses, cigarette filters, LCD panels, or membranes, just to name a few (Bonifacio et al., 2023). Efforts so far have been focused on chemical recycling of cellulose acetate (Bracciale et al., 2024). Recently, it has been demonstrated that the process of hydrothermal carbonisation (HTC) can be successfully used to decompose cellulose acetates into organic compounds such as different carboxylic acids and hydroxymethylfurfural (HMF), which are subsequently turned into carbon-rich solids of spherical morphology (Ischia et al., 2025).

HTC is a process performed in liquid water at temperatures ranging between 180 and 260 °C and autogenous pressure, with a multitude of different possible applications (Acosta et al., 2024; Lombardi et al., 2024; Mlonka-Mędrala et al., 2022). The HTC of sugars is capable of producing spherical micro/nano-particles (Falco et al., 2013; Schonvogel et al., 2019; Wang et al., 2022), using HMF as a precursor, which is a product of the decomposition of glucose in hydrothermal conditions (Ischia et al., 2022). This mechanism shares some similarities with carbon black formation mechanisms, which use polycyclic aromatic hydrocarbons (PAH) precursors to form nuclei that exhibit surface growth, followed by agglomeration (Okoye et al., 2021).

Interestingly, waste bioplastics, such as cellulose acetates, could also form microspheres in a similar manner as, in hydrothermal conditions, they undergo deacetylation to cellulose, which in turn is decomposed to glucose in acidic conditions, and subsequently forms HMF, a precursor for microspheres formation (Ischia et al., 2025).

HTC could thus be an attractive candidate for the production of carbon black-like material.

This work assesses a novel, environmentally friendly method for the production of carbon black-like material using waste bioplastic, namely cellulose acetate, as a feedstock, without the need to use fossil fuels or fossil-based feedstocks. Only a scarce amount of work has been dedicated so far to the production of carbon black, using biogenic feedstocks. These works focused on using pyrolysis oil from biomass pyrolysis (Toth et al., 2018; Wennebro et al., 2025). Carbon black production process relied in those cases on atomisation of the biooil (Toth et al., 2018; Wennebro et al., 2025). The production route investigated within the scope of this work involves HTC and pyrolysis. HTC creates microspheres (hydrochars), providing spherical particles prior to the pyrolysis process. Only a scarce amount of works has been dedicated to the characterisation of such hydrochars after pyrolysis (Wortmann et al., 2023, Wortmann et al., 2022). These works focused on hydrochars from HTC of model compounds, i.e., monosaccharides (glucose) and disaccharides (sucrose and trehalose). This work uses real bioplastic waste, and characterisation is focused on assessing the subsequent application of pyrolysed microspheres as a possible carbon black substitute. Such upcycling of waste bioplastics has never been investigated in the literature before. The goal of this work is to assess such a method (TRL 2–3) in terms of the potential applicability of the product and possible improvements in terms of environmental impacts, thus providing a proof of concept.

2. Materials and methods

2.1. Feedstock and samples

The feedstock used in this investigation is cellulose diacetate (CDA), provided both in blocks and milled form, supplied from an industrial partner (eyewear sector).

Across the manuscript, samples of cellulose diacetate are marked as CDA, hydrochars are marked as HC, whereas samples of hydrochars after pyrolysis are denoted as PYRO-500, PYRO-600, PYRO-700, and PYRO-900 depending on the pyrolysis temperature (500, 600, 700, and 900 °C, respectively).

2.2. Hydrothermal carbonisation

The HTC experiments were conducted using an autoclave vessel with a nominal volume of 2 L (Fig. S1). HTC of CDA blocks was performed at 250 °C, with a residence time of 1 h, since these conditions resulted in the highest yield of solids for HTC of CDA, as reported in the literature (Ischia et al., 2025). The feedstock to water ratio was 0.125, with 1.2 L of distilled water in the autoclave. Measurement of the residence time started after reaching a temperature 1 °C lower than the setpoint temperature (250 °C).

2.3. Pyrolysis

Pyrolysis was performed using a Carbolite Gero TF1-1200 furnace, with a quartz tube (Fig. S2). Pyrolysis of hydrochars was performed at 500, 600, 700, and 900 °C, with heating rate of 7 °C/min, followed by 1 h hold period (nitrogen flow of 150 cm^3/min). The mass of the sample boats and samples was determined using a Mettler Toledo ML204 balance with a maximum weight of 220 g and a resolution of 0.1 mg.

2.4. Analytical methods

Scanning electron microscopy (SEM) observations of hydrochars, pyrolyzed hydrochars, and commercial carbon black samples were performed using a Zeiss Supra 40 field emission scanning electron microscope (Carl Zeiss SMT GmbH) operating in vacuum at 10^{-6} Torr, equipped with a secondary electron detector and working at an acceleration voltage of 2.5 kV.

The porous structure was characterised by low-pressure gas adsorption analysis (details in supplementary materials). Iodine number determination was performed to obtain a performance metric typical of commercial carbon black (details in supplementary materials).

The chemical modification induced on the hydrochar by the pyrolysis treatment, i.e. the rearrangement of chemical bonds due to the loss of oxygen- and hydrogen-containing species, was investigated by X-ray photoelectron spectroscopy (XPS) (details in supplementary materials). Methods for elemental analysis (CHNO and ash determination), differential scanning calorimetry (DSC), and thermal analysis (both thermogravimetric analysis (TGA) and simultaneous thermal analysis (STA)), as well as FTIR for gases from STA and solids are included in supplementary materials. Detailed description of the assumptions made during calculation of mass and energy balances, and estimation of CO_2 footprint of the novel product are provided in the supplementary materials.

3. Results

3.1. Determination of optimum process conditions for production of HC-derived carbon black-like material

Derivative thermogravimetric (DTG) curves (Fig. 1) show clear differences between raw CDA blocks and the obtained hydrochar. The two clear and sharp peaks occurring between 300 and 400 °C in the DTG

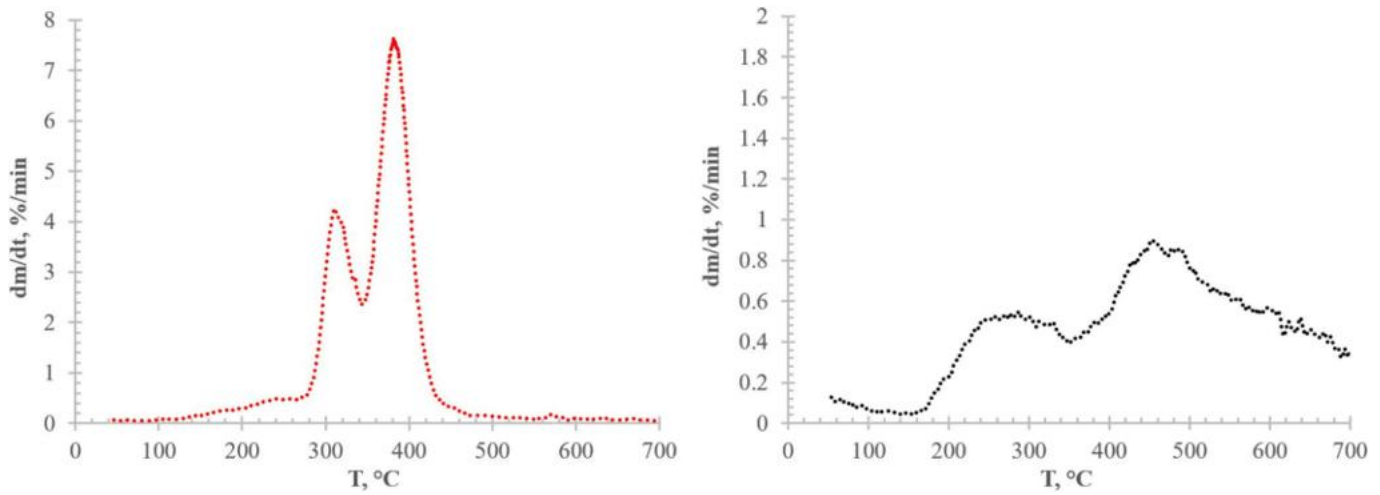

Fig. 1. DTG curve obtained in inert atmosphere (N_2) for CDA blocks (left) and hydrochars (right) produced by HTC of CDA blocks at 250 °C with a residence time of 1 h.

curve obtained for CDA in N_2 (Fig. 1 – left) are replaced by two less distinct peaks for hydrochar (Fig. 1 – right). The second peak observed for CDA within the scope of this study is well in line with the DTG peak observed for cellulose acetate (Feng et al., 2024), who, conversely, did not observe the first DTG peak at 300 °C. Such behaviour could be attributed to differences in terms of additives used, as thermal degradation of cellulose acetate can be influenced by additives (Boulven et al., 2019), and the CDA used in this investigation contains 40 % acetyl triethyl citrate (Ischia et al., 2025).

The first wide peak for hydrochar occurs at a lower temperature (approx. 250 °C) in comparison to the first peak for CDA (approx. 300 °C). One explanation could be that it is simply a remnant of the shoulder present at that temperature for CDA (Fig. 1 – left). However, a previous study has shown that cellulose diacetate can be hydrolysed almost completely in HTC at temperatures as low as 190 °C (Ischia et al., 2025). Moreover, solvent extraction of HCs after HTC of cellulose resulted in the removal of organic compounds adsorbed on the HC surface, such as carboxylic acids, furans, and furfurals (Ischia et al., 2023). Similarly, the possibility of freeing up additional surface by performing the extraction of the HC from the HTC of the organic fraction of municipal solid waste using acetone and methanol has been demonstrated by other works (Lucian et al., 2018). Thus, the first wide peak for hydrochar at low temperature (approx. 250 °C) could be attributed to the devolatilization of such adsorbed chemical species (Fig. 1).

When comparing HC to CDA, the second DTG peak lost its intensity and appeared at a slightly higher temperature (approx. 450 °C for hydrochars and 400 °C for CDA). HTC treatments typically turn the treated biomass into a more thermally resistant material, shifting the decomposition peak(s) towards higher temperatures (Mikusińska et al., 2025; Wilk et al., 2020). Such behaviour is usually attributable to a significant proportion of recalcitrant matter (e.g., lignin and cellulose), which determines a prevailing solid-to-solid conversion path. The main difference between these previous studies and the present investigation is that HTC of CDA causes a completely new material to form: CDA gets hydrolysed into the liquid phase, and then repolymerisation/condensation reactions occur and carbon microspheres form the so-called secondary char (Ischia et al., 2025; Shi et al., 2019; Wang et al., 2020), whose DTG decomposition peak is centred at approximately 450 °C (Yan and Li, 2015; Yu et al., 2012).

Considering the results of Fig. 1, increasing thermal stability necessary for obtaining a thermally stable carbon black-like material requires a pyrolysis temperature higher than the second detected DTG peak, i.e. a temperature of at least 500 °C, which indicated the temperature range selected for pyrolysis in the furnace.

The hydrochar yield from HTC of CDA at 250 °C with a residence time of 1 h in the 2 L reactor (18.3 %, Table 1), is in very good agreement with the hydrochar yield obtained in a previous work in a 50 cm^3 reactor at the same operating conditions (Ischia et al., 2025).

Performed pyrolysis experiments have shown that the mass yield of solids from the process stabilises around 700 °C at a value of 54 % (Table 1). The yield of a single-stage process (pyrolysis of CDA) has not been determined, as preliminary experiments have shown that pyrolysis of CDA is not capable of producing spherical carbon black-like particles, producing flat sheets of carbonised material instead with no observable aciniform structures (Fig. S4).

Details of residual weight at selected TGA temperatures are reported in Table 1. Small differences might be caused by non-uniformity in particle sizes, possibly influencing the heat exchange between the sample and the surrounding atmosphere. Such heat exchange is important (Czajka, 2021). TGA of hydrochars resulted in mass loss of approximately 40 % at 700 °C (Table 1), which is in good agreement with the mass loss observed by other studies during TGA of hydrochars produced from glucose (Wortmann et al., 2023).

Observed thermal stability (Table 1) for PYRO-700 (95.9 %) and PYRO-900 (97.6 %) is well in line with reported 95 % fixed carbon content reported in the literature for carbon black recovered by pyrolysis (Fadipe et al., 2025). Looking at the heat of pyrolysis obtained by the DSC (Table 1), the process is endothermic up to 600 °C. However, the process clearly becomes exothermic at higher temperatures. On the one

Table 1
Solid mass yields of HTC and pyrolysis, TGA mass loss for selected temperature (Ym – mass yield; m_{250}, m_{350}, m_{500}, m_{600}, and m_{700} indicate residual mass after 250, 350, 500, 600, and 700 °C, respectively; % weight reported for yields and residual mass; Q – heat for pyrolysis, negative value indicates endothermal process).

	Ym		m_{250}	m_{350}	m_{500}	m_{600}	m_{700}	Q
Sample:	**%**		**%**	**%**	**%**	**%**	**%**	**MJ/kg**
CDA blocks	–	–	93.5	59.8	11.7	10.3	9.3	–
CDA milled	–	–	94.5	59.6	11.1	9.3	7.6	–
HC	18.3	±0.4	94.8	88.0	72.8	64.1	58.1	–
PYRO-500	64.5	±0.5	99.3	99.7	98.0	91.2	80.3	– 0.25
PYRO-600	58.8	±0.8	99.3	99.2	98.7	97.1	92.5	– 0.14
PYRO-700	53.9	±0.1	99.2	99.8	98.8	97.8	95.9	0.32
PYRO-900	54.0	±0.1	99.9	99.1	99.3	98.4	97.6	2.49

hand, exothermic process seems beneficial from the energy perspective. On the other hand, the risk of exothermal runaway would complicate reactor design.

XPS confirmed that the pyrolysis treatment causes a drastic reduction in the O content and carbonisation of the samples, while data obtained via traditional elemental analysis would seem to contradict this (Table S1 and relevant critical discussion in supplementary material). The surface abundance of chemical bonds obtained from fitting XPS data is reported in Table 2. Hydrochars after pyrolysis became increasingly aromatic, as indicated by increased share of C=C (sp^2) type bonds and correspondingly decrease of C–C (sp^3) bonds (Table 2). C 1 s part of spectra (Fig. S6) were fitted with up to eight lines from which first line lies at a binding energy of 284.4 eV, indicating C=C (sp^2) type bonds (Beamson and Briggs, 1993). The second line at 285.0 eV indicates C–C (sp^3) bonds (Beamson and Briggs, 1993; Rouxhet and Genet, 2011), the third line at 286.0 eV points out the existence of C-OH and/or C-O-C type bonds (Beamson and Briggs, 1993; Rouxhet and Genet, 2011), the fourth line at 287.1 eV indicates presence of C=O and/or O-C-O type compounds, whereas the fifth line at 288.3 eV shows O-C=O bonds (Beamson and Briggs, 1993; Rouxhet and Genet, 2011), the sixth line found at 289.7 eV indicates presence of either shake-up satellite and/or O-(C=O)-O type groups and, finally, the lines at 291.1 and 293.1 eV come from shake-up satellites (Briggs, 2005). Shake-up excitation originates from the sp^2 carbon and its aromatic forms and is an additional parameter confirming the presence of this type of bond (Beamson and Briggs, 1993).

For all samples, the O 1 s spectra were fitted with two lines, with the first one centred at 531.6 eV, which indicates O=C type bonds and the second line at 533.3 eV, which indicates the presence of O-C and/or –OH bonds (Wagner et al., 2003). Apart from C and O, also marginal amounts of K and Na were detected during the analysis, likely artefacts from the sample boats used for the pyrolysis. C 1 s and K2p lines overlap and are presented on the same plot (Fig. S6). No other elements were detected within the XPS detection limit (~ 0.1 at. %).

Thermal analysis coupled with FTIR has shown that hydrochars (Fig. S8) during pyrolysis produce permanent gases (CO, CO_2, CH_4), as well as condensable compounds such as acetic acid, which are typically detected for pyrolysis of various organic feedstocks (Sieradzka et al., 2020; Wang et al., 2021; Wen et al., 2021). The release of acetic acid first peaked at approximately 200 °C, which is typically recognised as the lower end of the torrefaction regime (Luo et al., 2022; Piersa et al., 2022; Szufa et al., 2025). This indicates that acetic acid released during the first peak might have been adsorbed on the surface of hydrochars (Ischia et al., 2023) and subsequently desorbed during heating. It seems plausible to attribute the second acetic acid peak to pyrolysis and to some extent decomposition of heavier compounds, as some works on TG-FTIR of organic materials attributed organic acids as secondary products (Junga et al., 2024). Interestingly, thermal treatment of hydrochars produced using CDA starts forming water at approximately 250 °C, which ensures that it is not an effect of drying, and the concentration of this thermal decomposition product steadily increases all the way to 900 °C. During the thermal treatment of CDA-based hydrochars pyrolysed at 500 °C (Fig. S8), only CO and CH_4 were detected with an almost parallel profile in the Gram-Schmidt curves, and at relatively similar concentrations in comparison to pristine hydrochars. Two peaks can be observed for both gaseous products. It seems plausible to attribute such behaviour to decomposition of different pyrolysis products present in the sample, with the second peak attributable to decomposition of more thermally stable compounds. Further research is recommended concerning production of other condensable compounds, especially those problematic from application perspective, such as tars.

3.2. Comparison of the HC-derived carbon black-like material with commercially available product

Key parameters for commercial carbon black are its morphology and surface area (Melsom, 2003). Desired morphology is so-called high structure, which could be observed directly by SEM or inferred indirectly based on the oil absorption number, typically determined during quality control (Melsom, 2003) and also important for its classification (D1765-23b).

SEM images (Fig. 2) show a comparison between the morphology of a commercial carbon black (Fig. 2 – A), CDA-based hydrochars (Fig. 2 – B), and produced carbon black-like material (Fig. 2 – C, D, E, F). Hydrochars obtained after HTC of cellulose diacetate (250 °C, 1 h) show a typical spherical morphology, similar to hydrochars after HTC of glucose (Ischia et al., 2022). The morphology of the particles obtained by pyrolysis of hydrochar resembles commercial carbon black much more than hydrochars without pyrolysis (Fig. 2), showing predominantly the high structures of carbon black, which typically have aggregates with smaller particles and a more branched shape (Jianwen et al., 2004; Neffati and Brokken-Zijp, 2021), described in the ASTM D3053 – 23a standard (Standard Terminology Relating to Carbon Black) as an aciniform morphology. According to the ASTM D3053-23a standard, the spheroidal primary particles of carbon black are typically fused into aggregates of colloidal dimension, which, from a morphological perspective, is characteristic of such a product. According to IUPAC recommendations, colloidal dimensions range between 1 nm and 1 μm (Slomkowski et al., 2011).

SEM images of carbon spheres (hydrochar or, more precisely, secondary char) obtained within the scope of this study suggest a similar particle size (mostly between 1 and 10 μm – see Fig. 2B) to hydrochars produced using glucose (Elaigwu and Greenway, 2016; Ischia et al., 2022). Their morphology generally resembles hydrochars produced from different sugars (Ubene et al., 2024). After pyrolysis, carbon spheres tend to decrease in dimensions, with a significant number of particles within the colloidal dimension range, even if such a generalist behaviour is contradicted by some larger spheres, which still remain after the pyrolytic treatment. Particle size visible within the structure of commercial carbon black was generally smaller in comparison to the particles obtained by pyrolysis of hydrochars. Nonetheless, high structures with aciniform morphology could be observed for both commercial carbon black and the pyrolysed HC (Fig. 2). Such high structures are typical for carbon black (Melsom, 2003; Neffati and Brokken-Zijp, 2021) and are one of the important aspects concerning its designation (Melsom, 2003). This suggests that further work is required on

Table 2
Bonds abundance (%) determined by fitting XPS spectra.

	C								O	
Binding energy, eV	**284.4**	**285.0**	**286.0**	**287.1**	**288.3**	**289.7**	**291.1**	**293.0**	**531.6**	**533.3**
Groups / Oxidation state	**C=C sp^2**	**C–C sp^3**	**C-O-C; C-OH**	**O-C-O; C=O**	**O-C=O**	**O(C=O)O shk-up**	**shk-up**	**shk-up**	**O=C**	**O-C**
HC	18.8	50.7	8.5	0.0	3.8	0.8	0.0	0.0	8.3	9.2
PYRO-500	57.3	17.6	6.9	2.8	3.4	2.3	0.2	1.3	1.9	6.3
PYRO-600	66.8	12.5	6.1	3.7	3.6	1.7	1.7	0.0	1.0	3.1
PYRO-700	59.7	14.8	0.0	5.8	4.3	3.7	3.5	2.9	2.5	2.5
PYRO-900	58.5	18.6	4.3	4.2	3.1	3.6	2.8	1.7	1.8	1.1

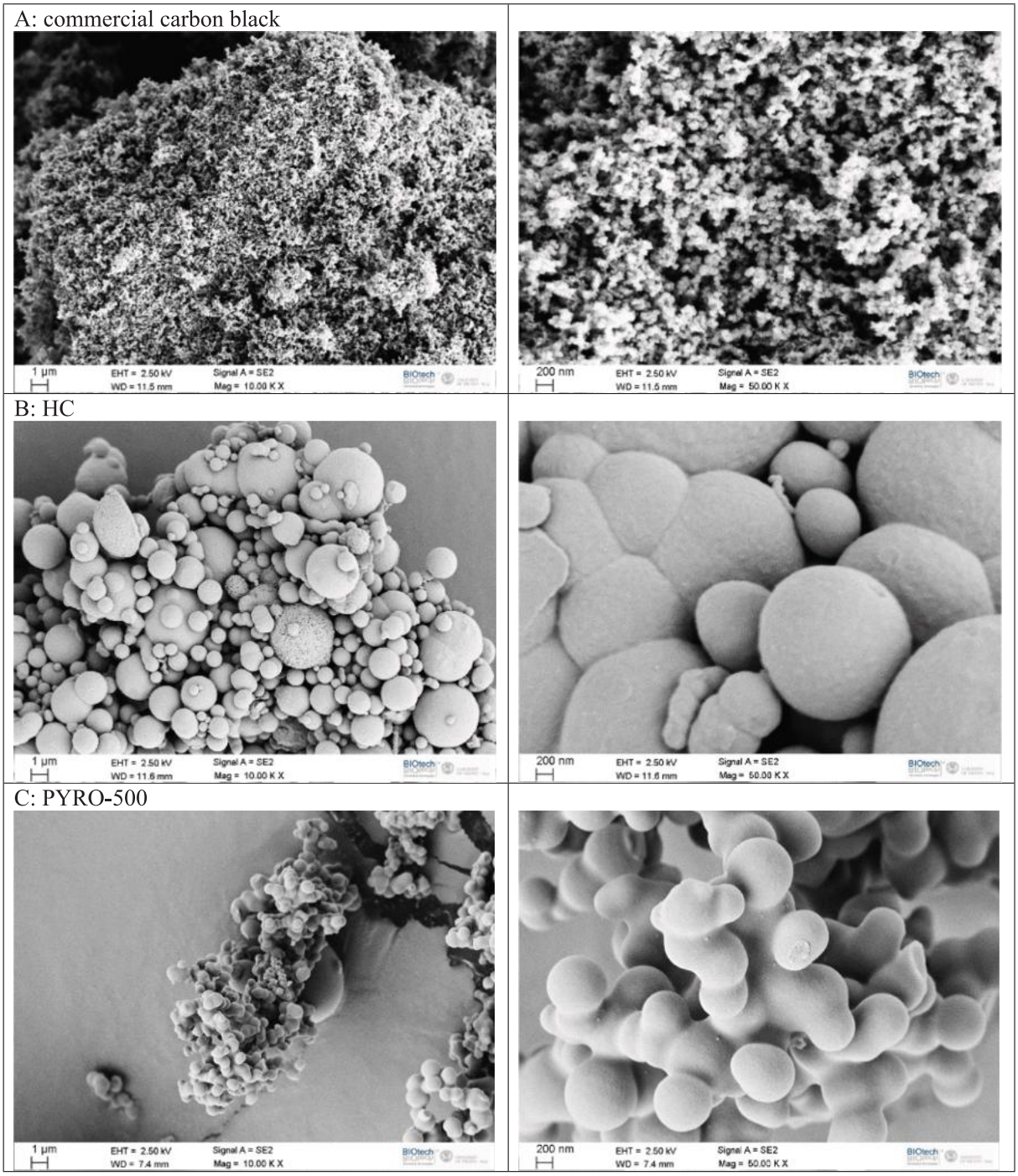

Fig. 2. A: SEM images at different magnifications: 10,000 (left), and 50,000 (right).

optimisation of the particle size of HC-derived carbon black-like product, as the mechanism is still not well understood, whereas, much better understanding has been achieved for controlling the particle size of the state-of-the-art fossil-based carbon black (Kelesidis et al., 2023).

The decrease in the size of spherical particles after pyrolysis of HC, as observed by SEM (Fig. 2), could be caused by devolatilization of the particles' shell. Literature reports that carbon spheres formed during the HTC of saccharides, such as cellulose, consist of a hydrophobic core and hydrophilic shell (Sevilla and Fuertes, 2009a,b). Similarly, a core–shell structure has been reported for carbon black (Kelesidis et al., 2024). The density of the hydrochars increases after pyrolysis (Table S1), which suggests that the density of the core might be higher than the density of the shell. The decrease in the density after pyrolysis at 900 °C could be attributed to thermal expansion typical of expanded graphite (Qureshi et al., 2018; Taherian, 2018).

Surface area can be determined directly by nitrogen adsorption, or could be inferred indirectly by measuring iodine number, as established correlations exist for carbon black between the two parameters (Melsom, 2003). Analysis of low-pressure nitrogen adsorption revealed that the porous structure of the pyrolysed samples differed significantly depending on the applied temperature (Fig. 3). The adsorption isotherm of the sample pyrolysed at 600°C exhibited type I behaviour, closely

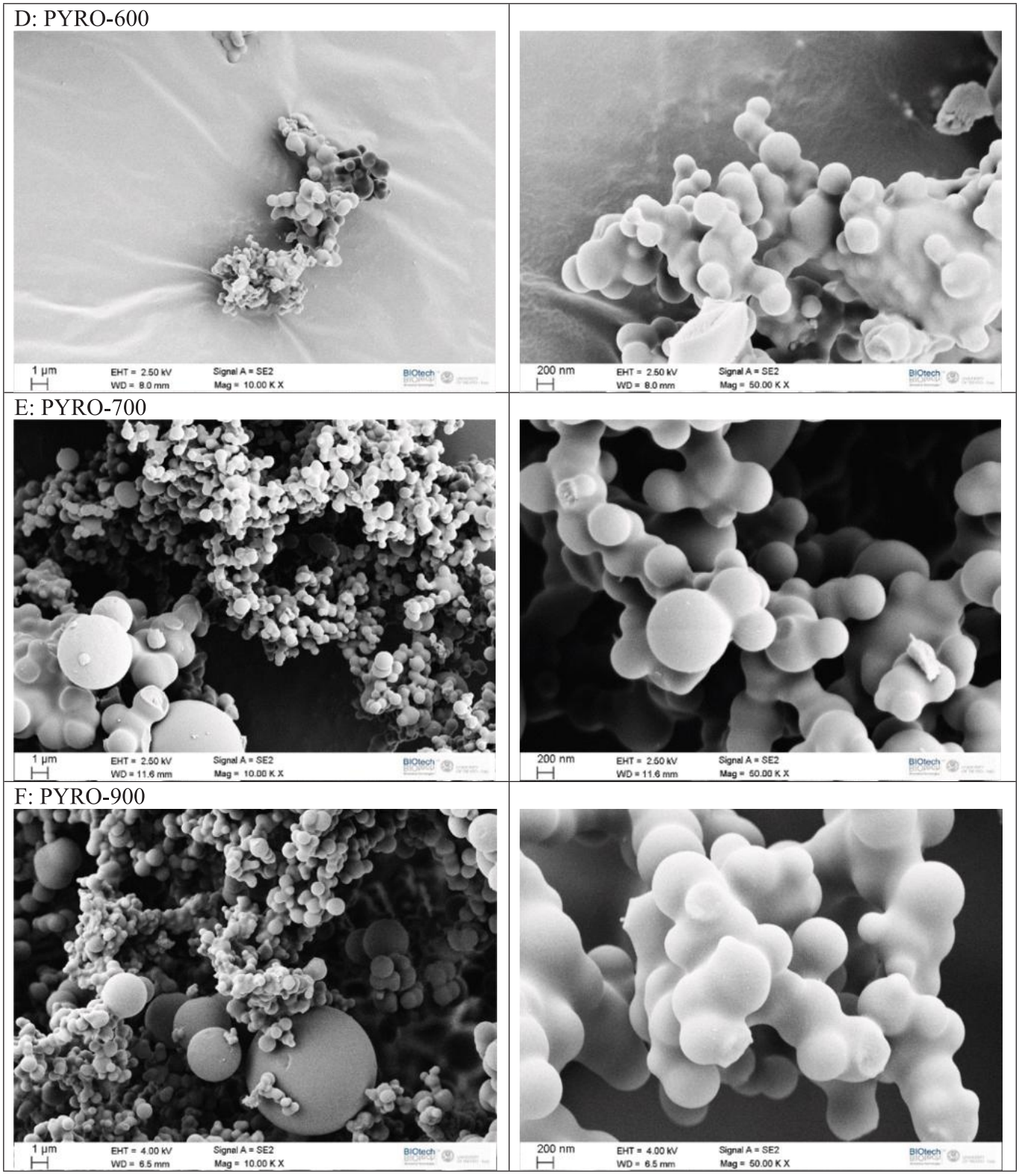

Fig. 2. (*continued*).

resembling the Langmuir isotherm, which is characteristic of materials with well-developed microporosity. The most intensive filling of sorption sites occurred here at low relative pressures (0–10 kPa), corresponding to micropore filling. In contrast, the sample pyrolysed at 500 °C displayed a type II isotherm, similar in shape to the BET isotherm, while the other samples exhibited type III isotherms, typical for non-porous materials. Such type III isotherms characteristic of HC, PYRO-700 and PYRO-900 overlap in Fig. 3. No evidence of increased adsorption due to capillary condensation—associated with the filling of larger mesopores—was observed in any of the samples. Each time, the desorption curve also did not reproduce the course of the adsorption isotherm, indicating a delayed mechanism of pore emptying. Structural

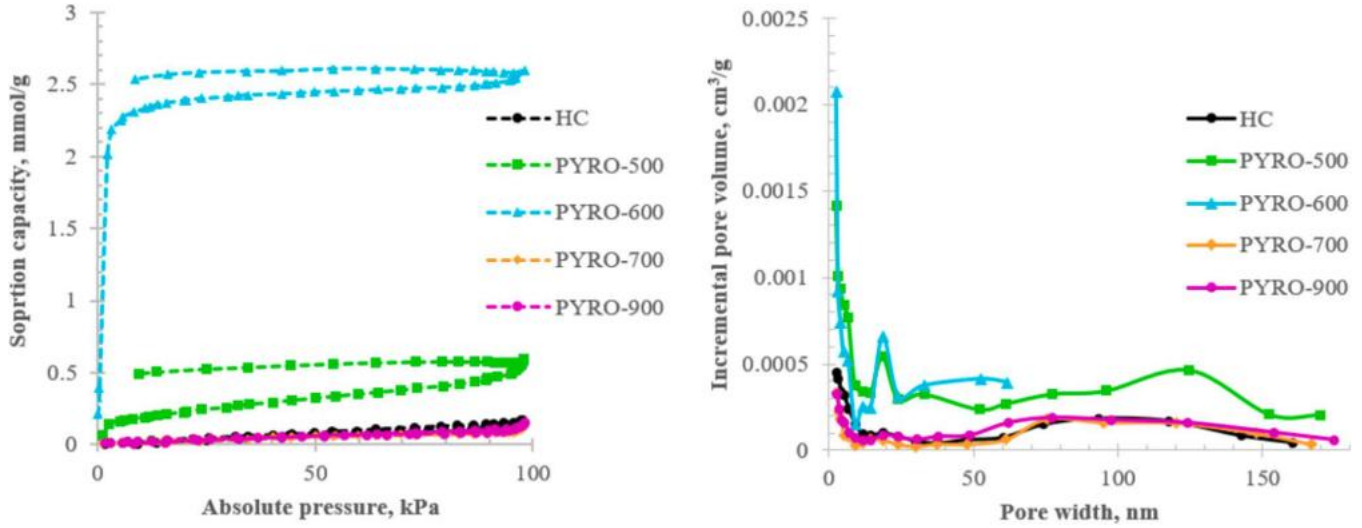

Fig. 3. Left: Nitrogen adsorption isotherms of hydrochar and hydrochars pyrolysed at different temperatures; Right: Pore size distribution of hydrochar and pyrolysed hydrochars according to BJH model.

parameters were determined based on adsorption points, and the results are presented in Table 3.

According to the results (Table 3), the hydrochar sample exhibited a low degree of porosity. The structural parameters were minimal, with a specific surface area of 5.1 m^2/g (SA_{BET}) and a pore volume of 6.3 × 10^{-3} cm^3/g (V_{BJH}) (Table S2). Such hydrochar retains a relatively large amount of organic matter and volatile components (41.9 %, Table 1). The pore structure is poorly developed, and the SA_{BET} is low because the pores are blocked by residual volatiles. This is consistent with other research results (Sevilla and Fuertes, 2009a; Tran et al., 2018). After pyrolysis at 500 °C (PYRO-500), the previously closed pore space gradually opened in the non-porous HC structure. This is the result of the release of volatile fractions, promoting the gradual opening of previously closed pore channels. Based on pore space analysis using traditional models (BET, BJH), new fine pores with diameters < 10 nm and 15–25 nm were formed in PYRO-500, and the pore volume increased to approximately 17 × 10^{-3} cm^3/g (Fig. 3). This led to an increase in the SA_{BET} to 18.4 m^2/g. A similar trend was also observed by other authors (Abdoul Magid et al., 2021; Fu et al., 2022). The most intense expansion of the pore structure in the mesopore region occurred in the PYRO-600 sample. The applied temperature resulted in the formation of a system of fine pores with diameters of 18–25 nm (Fig. 3) and an increase in the volume of the micropores (V_{DFT}) to 82.6 × 10^{-3} cm^3/g (Table 3). In the mesopore range (BJH), increased volume was observed in pores with a diameter of 20 nm (Fig. 3), and the total mesopore volume was 9.6 × 10^{-3} cm^3/g. The specific surface area of SA_{BET} reached 175.4 m^2/g. This is well in line with the surface area for carbon black-like material recovered after tyre pyrolysis at 600 °C, which was reported to be 190 m^2/g (Fadipe et al., 2025). Further increase in pyrolysis temperature (PYRO-700, PYRO-900) resulted in collapse and sealing of the pore structure. These samples were nonporous and had structural parameters similar to the initial sample HC. Consequently, transport paths for the adsorbate became inaccessible, and the specific surface area decreased drastically. According to the presented structural studies, the optimal temperature range for opening the transport channels for the adsorbate was 600 °C.

Iodine adsorption number is also important from the point of view of classification of carbon black (D1765 − 23b). The raw hydrochar microspheres exhibited a relatively low iodine number (IN < 330 mg/g), in comparison to pyrolysed samples (Table 3). After pyrolysis at 500 °C, IN remained essentially unchanged (318 ± 13 mg/g), but a progressive increase was observed at 600 °C (464 ± 59 mg/g) and a maximum at 700 °C (488 ± 17 mg/g). At 900 °C, IN decreased slightly (457 ± 25 mg/g), indicating that excessive severity of pyrolysis can deteriorate the porous structure of pyrolysed hydrochars. Interestingly, the range of IN reported for carbon black obtained from pyrolysis of waste tyres could be as low as 94–118 mg/g (Thonglhueng et al., 2022). Recovered carbon black with such IN can reportedly still be used as a filler in rubber compounds (Thonglhueng et al., 2022), close to carbon black with N330 designation (Melsom, 2003; Thonglhueng et al., 2022).

Comparison of the carbon black-like material, obtained within the scope of this study, with different commercial types of carbon black provides some indications regarding applicability, including possibilities of at least partial substitution (Table 3). Firstly, it is important to highlight that a wide variety of products exists on the market, aiming at different applications. Among the commercial carbon black, listed in ASTM D1765-23b standard (Standard Classification System for Carbon Blacks Used in Rubber Products), surface areas vary between 8 and 143 m^2/g (Table 3). In fact, ASTM D1765-23b also mentions the possibility of designation in group 0 for carbon black with surface area > 150 m^2/g. The BET surface area of a commercial carbon black, used for the purpose of comparing the morphology with the samples obtained within the scope of this study (Vulcan XC-72), has been reported in the literature to range between 245 and 254 m^2/g (Table 3). Some samples of carbon black, such as Printex XE-2 or Black Pearl 2000, reach surface areas < 1000 m^2/g, making them comparable with activated carbon (Table 3). Surface area obtained for the sample of hydrochars after pyrolysis at 600 °C reached a surface area of 175.4 ± 3.9 m^2/g, which places the novel product within the range reported for lower-tier commercial products (Table 3). A similar statement could be made concerning achieved iodine adsorption numbers. However, in this case, it should be noted that many literature sources (other than industrial standards or commercial leaflets) simply do not report the iodine number (Table 3), likely because both BET and iodine adsorption number aim at quantification of the surface area (Melsom, 2003). Similarly, micropore volume is scarcely reported for commercial samples of carbon black (Table 3), and reported values can vary by as much as three orders of magnitude, since Furnace black reportedly achieved a micropore volume of 0.003 cm^3/g, whereas Black Pearls 2000 was able to reach 0.590 cm^3/g (Table 3). This puts into context the micropore volumes of carbon black-like samples obtained within the scope of this study, which ranged between 0.083 and 0.002 cm^3/g for the samples after pyrolysis at 600 and 900 °C, respectively (Table 3). Further validation of the novel product in particular applications, e.g., as a filler/reinforcement, could shed more light on the equivalence of the obtained carbon black-like product with commercially available carbon black. Such a validation would require upscaled production but could also bring the novel

Table 3
Comparison between novel carbon black-like material produced within the scope of this study and commercial carbon black with different designations, as well as other novel technologies for carbon black production (plasma conversion of natural gas and partial oxidation of spent tyre pyrolysis oil).

Sample	Iodine Adsorption Number mg/g	BET surface area m^2/g	Micropore volume cm^3/g	Reference
HC	327 ± 46	5.1 ± 0.1	0.003	this study
PYRO-500	318 ± 13	18.4 ± 0.2	0.017	this study
PYRO-600	464 ± 59	175.4 ± 3.9	0.083	this study
PYRO-700	488 ± 17	4.1 ± 0.1	0.002	this study
PYRO-900	457 ± 25	3.5 ± 0.1	0.002	this study
N110	145	127	n.d.	ASTM D1765-23b
N110 (from Cabot)	130	n.d.	n.d.	(Kiani et al., 2023)
N134	142	143	n.d.	ASTM D1765-23b
N134 (Corax from Evonik)	n.d.	159	n.d.	(Onyeka Okoye et al., 2022; Strzemiecka et al., 2014)
N220	121	114	n.d.	ASTM D1765-23b
N220 (Corax from Evonik)	n.d.	178	n.d.	(Onyeka Okoye et al., 2022; Strzemiecka et al., 2014)
N326	82	78	n.d.	ASTM D1765-23b
N326 (Corax from Evonik)	n.d.	71	n.d.	(Onyeka Okoye et al., 2022; Strzemiecka et al., 2014)
N330	82	76	n.d.	ASTM D1765-23b
Vulcan XC-72 (N472)	n.d.	245–254	0.060	(Pantea et al., 2003, 2001)
N550	43	40	n.d.	ASTM D1765-23b
N660	36	35	n.d.	ASTM D1765-23b
N660	n.d.	33.2 ± 0.6	n.d.	(Williams et al., 2023)
N750	27	27	n.d.	ASTM D1765-23b
N774	29	30	n.d.	ASTM D1765-23b
N774 (Corax from Evonik)	n.d.	32	n.d.	(Onyeka Okoye et al., 2022; Strzemiecka et al., 2014)
Thermal black	n.d.	13	n.d.	(Pantea et al., 2003)
	n.d.	6–15	n.d.	(Okoye et al., 2021)
Furnace black	n.d.	99	0.003	(Pantea et al., 2003)
	15–450	12–240	n.d.	(Okoye et al., 2021)
Plasma carbon black	213	n.d.	n.d.	(Cho et al., 2004)
Conductex SC	n.d.	190	0.030	(Pantea et al., 2003)
Conductex 975	n.d.	250	0.050	(Pantea et al., 2003)
Printex L	n.d.	150	0.040	(Pantea et al., 2003)
Printex L6	n.d.	190	0.040	(Pantea et al., 2003)
Printex XE-2	n.d.	1300	0.030	(Pantea et al., 2003)
Black Pearls 2000	n.d.	1635	0.590	(Pantea et al., 2003)
Graphitised black	n.d.	33	n.d.	(Pantea et al., 2003)
Partial oxidation of spent tyre pyrolysis oil	n.d.	19–21	n.d.	(Onyeka Okoye et al., 2022)
Cancarb N880	n.d.	12.3	n.d.	(Pantea et al., 2001)
Asahi N880	n.d.	25.4	n.d.	(Pantea et al., 2001)
Sichuan Southwest Longchang N880	n.d.	13.8	n.d.	(Pantea et al., 2001)
Cancarb N990	n.d.	10.3	n.d.	(Pantea et al., 2001)
Cancarb N990 UP	n.d.	9.7	n.d.	(Pantea et al., 2001)
Columbian Chemicals Co. N990	n.d.	7.6	n.d.	(Pantea et al., 2001)
Cancarb N991	n.d.	9.5	n.d.	(Pantea et al., 2001)
Severgazprom N991	n.d.	9.8	n.d.	(Pantea et al., 2001)

bioplastics upcycling method to a higher TRL (TRL4 – technology validated in laboratory conditions).

3.3. Sustainability of the proposed production path

Sustainability is one of the issues of state-of-the-art carbon black production, due to the use of fossil fuels for its production. In conventional plant with flaring of the tail gas, specific CO_2 emissions per kg of carbon black can be as high as 3.50 kg_{CO2}/kg (Rosner et al., 2024). This is clearly the worst-case scenario, as literature also reports lower values, i.e., 3.01 kg_{CO2eq}/kg (Wu et al., 2024). Nonetheless, it is hard to overlook the large room for potential improvement. The production method analysed in this work is based on the use of biogenic waste, which could be considered neutral from a climate change perspective (Cherubini et al., 2011; Materazzi et al., 2024). Moreover, assessing the environmental impacts of waste often involves the assumption that the waste is burden-free (cut-off approach), which seems sensible, since it is the product, not the waste, that is responsible for the emissions (Rossi et al., 2025; Wang et al., 2023). In the case of the technology assessed within the scope of this study, energy balance is of the utmost significance, as the environmental performance of the HTC process is primarily connected with its energy consumption (Lombardi et al., 2023). The energy balance for the novel technology assessed within the scope of this study is shown in Fig. 4. As shown by the energy balance, production of the carbon black-like material is not autothermal and requires an external energy supply. However, it should be noted that such consumption is already minimised by the recovery of sensible heat, which is a typical practice in HTC technologies (Ferrentino et al., 2023). Moreover, chemical energy from the liquid products of HTC could be recovered by anaerobic digestion, along with subsequent combustion of the produced biogas (Aragón-Briceño et al., 2017; De la Rubia et al., 2018; Gomes et al., 2021). Liquid products from HTC of CDA have also been shown to produce biogas in thermophilic conditions (Marchelli et al., 2023). In fact, methane in the biogas produced from liquid products of HTC of 1000 kg of CDA contains 1057 MJ of chemical energy (LHV-based), which is 25 % of the chemical energy input to the CHP (Fig. 4). Overall, two scenarios were assumed in the assessment regarding the supply of

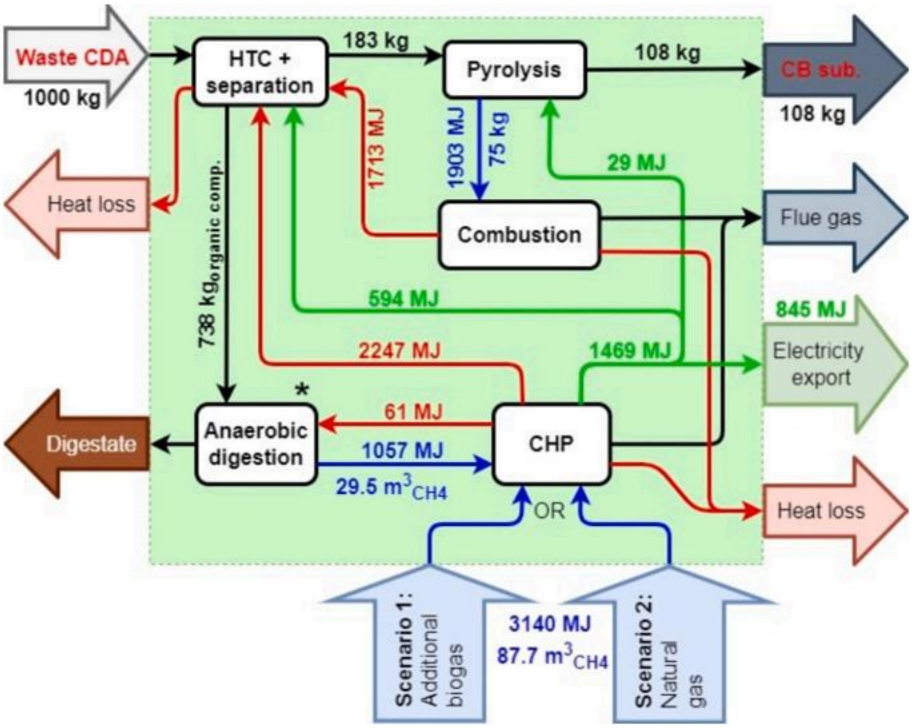

Fig. 4. Mass and energy balance of the novel technology for bioplastic waste (CDA) utilisation, consisting of HTC and pyrolysis, along with other auxiliary modules (* – mechanical dewatering of the digestate and recirculation of the liquid back to HTC, not shown for simplicity).

additional energy, i.e., scenario 1 involved additional biogas supplied from a bigger anaerobic digestion unit and scenario 2 involved supplying additional natural gas to the CHP unit (Fig. 4). Scenario 1 is relevant for the cases in which the source of cellulose acetate waste is located closely to biogas plants, which is especially likely taking into account the fact that processing of municipal waste streams often involves anaerobic digestion (Colazo et al., 2015; Seruga et al., 2025). Moreover, possibilities of integration of HTC and anaerobic digestion were demonstrated for waste streams such as sewage sludge (Hämäläinen et al., 2024), or digestate from the organic fraction of municipal solid waste (Aragon-Briceño et al., 2022), thus providing indications of applicability of such approach in many cases.

Performed analysis shows that CO_2 equivalents of products from Scenario 1 and Scenario 2 improve with respect to literature data for carbon black. Climate change impact has been assessed as 0.49 and 1.79 kg_{CO2eq} per kg of product for Scenario 1 and Scenario 2, respectively. Even though the performance of such a product in applications typical of carbon black (e.g., reinforcing filler for rubbers or plastics) has not been proven so far, it seems plausible to assume that at least partial substitution is possible by looking at the comparison provided in Table 3. Even a 10 % substitution by mass would allow for a decrease of the climate change impact, in comparison to state-of-the-art carbon black (Fig. 5).

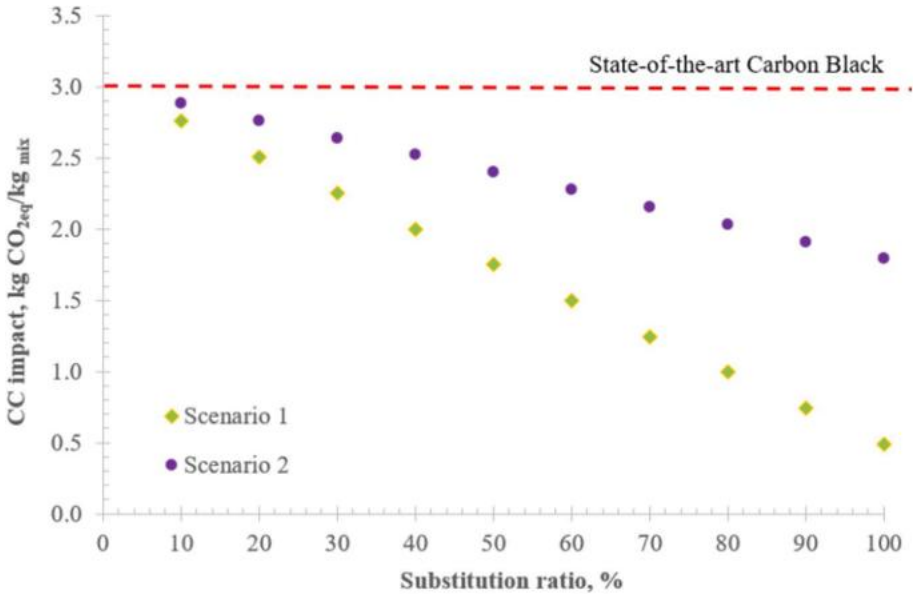

Fig. 5. Climate change impact considering the use of the new carbon black-like material mixed with commercial carbon black in different proportions. Biogas and natural gas refer to Scenario 1 and Scenario 2, respectively.

Moreover, higher substitution ratios of the product for the case of Scenario 1 could make environmental performance competitive in comparison to other novel sustainable solutions. Integrated technology recovering carbon black from waste tyres and producing additional carbon black using the waste tyre pyrolysis oil (InTech) was reported to decrease the global warming impact by 1.59 kg_{CO2eq} in comparison to conventional carbon black production (Wu et al., 2024). It could be noticed in Fig. 5 that similar environmental performance could be achieved by 70 % substitution using carbon black-like material produced using biogas only (Scenario 1).

It should not be overlooked that the performed analysis attributed all CO_{2eq} to the carbon black-like product, disregarding the fact that in both cases an additional 845 MJ of electricity would be generated (Fig. 5). A life cycle assessment (LCA) with proper allocation between the carbon black-like substitute and electricity would further decrease the environmental burden of the former by allocating a part of the burden to the latter.

Further experimental research is recommended, concerning possible substitution that could actually be achieved by the novel carbon black-like product in different applications. Moreover, future research is also recommended concerning the economic and social sustainability that could be achieved by combined HTC-pyrolysis installations producing such a carbon black-like substitute on a larger scale. Economic sustainability can be determined by techno-economic analysis. Furthermore, environmental sustainability investigation should be extended to other impact categories, fully implementing the LCA methodology.

4. Conclusions

Waste bioplastics can be converted into a carbon black-like material by a cascade of processes consisting of HTC and pyrolysis. Morphology of hydrochars upgraded by pyrolysis was similar to that of commercial carbon black and showed the presence of high structures. XPS testified a substantial carbonisation and aromatisation of the pyrolysed hydrochars. Hydrochars after pyrolysis at 700 °C contained only slight amounts of volatile matter (4.1 %), as shown by TGA. However, high temperatures of pyrolysis (700 and 900 °C) might not be considered favourable to hydrochars, due to the collapse of porous structures, resulting in decreased surface area and pore volume. For applications of carbon black requiring high surface area, it could be considered beneficial to perform pyrolysis at 600 °C. It seems sensible to recommend further studies focused on specific applications of the carbon black-like material produced using the proposed method, including the determination of achievable substitution ratios. This could provide definite answers regarding the applicability of carbon black-like material produced from bioplastic waste, using a cascade of processes consisting of hydrothermal carbonisation and pyrolysis. Performed preliminary analysis suggests excellent environmental performance of the novel carbon black-like material, with climate change impacts ranging between 0.49 and 1.79 $kgCO_{2eq}$ per kg of product, depending on the choices concerning the source of supplementary heat. An in-depth prospective life cycle assessment study of such a novel upcycling method of waste bioplastics is advised to confirm preliminary results and take into consideration other environmental impact categories.

CRediT authorship contribution statement

Lukasz Niedzwiecki: Formal analysis. **Luca Fambri:** Writing – review & editing, Validation, Resources, Methodology, Investigation, Formal analysis, Data curation. **Filippo Marchelli:** Writing – review & editing, Validation, Methodology, Investigation, Formal analysis, Data curation. **Anna Pajdak:** Writing – review & editing, Validation, Resources, Methodology, Investigation, Formal analysis, Data curation. **Marco Calvi:** Writing – review & editing, Resources. **Luca Fiori:** Writing – review & editing, Validation, Supervision, Resources, Project administration, Methodology, Funding acquisition.

Declaration of competing interest

The authors declare that they have no known competing financial interests or personal relationships that could have appeared to influence the work reported in this paper.

Acknowledgements

The authors would like to acknowledge the support provided by Ms. Claudia Gavazza with analysis of the samples (DSC, FTIR, TGA, SEM, STA and density), Prof. Narges Ataollahi for determination of the Iodine Number, Dr Eng. Mateusz Marzec for XPS analysis, and Ms. Wilma Waona for CHN analysis.

The authors thank Fondazione Cariverona for the financial support in the framework of the Occhio al Bio! project, funded within the Ricerca&Sviluppo 2020 call.

Appendix A. Supplementary material

Supplementary data to this article can be found online at https://doi.org/10.1016/j.wasman.2025.115308.

Data availability

Data will be made available on request.

References

Abdoul Magid, A.S.I., Islam, M.S., Chen, Y., Weng, L., Li, J., Ma, J., Li, Y., 2021. Enhanced adsorption of polystyrene nanoplastics (PSNPs) onto oxidized corncob biochar with high pyrolysis temperature. Sci. Total Environ. 784, 147115. https://doi.org/10.1016/j.scitotenv.2021.147115.

Acosta, A.C., Arias, C.A., Biller, P., Wittig, N.K., Baragau, I.A., Alhnidi, M.J., Ravenni, G., Sárossy, Z., Benedini, L., Abramiuc, L.E., Popescu, D.G., Negassa, W., Marulanda, V. F., Müller-Stöver, D.S., Brix, H., 2024. Hydrothermal carbonization and pyrolysis in wetland engineering: carbon sequestration, phosphorus recovery, and structural characterization of willow-based chars with X-ray μ-computed tomography. Chem. Eng. J. 492. https://doi.org/10.1016/j.cej.2024.151916.

Aragon-Briceño, C., Pożarlik, A., Bramer, E., Brem, G., Wang, S., Wen, Y., Yang, W., Pawlak-Kruczek, H., Niedźwiecki, Ł., Urbanowska, A., Mościcki, K., Płoszczyca, M., 2022. Integration of hydrothermal carbonization treatment for water and energy recovery from organic fraction of municipal solid waste digestate. Renew. Energy 184, 577–591. https://doi.org/10.1016/j.renene.2021.11.106.

Aragón-Briceño, C., Ross, A.B.B., Camargo-Valero, M.A.A., 2017. Evaluation and comparison of product yields and bio-methane potential in sewage digestate following hydrothermal treatment. Appl. Energy 208, 1357–1369. https://doi.org/10.1016/j.apenergy.2017.09.019.

Aylón, E., Fernández-Colino, A., Navarro, M.V., Murillor, R., García, T., Mastral, A.M., 2008. Waste tire pyrolysis: comparison between fixed bed reactor and moving bed reactor. Ind. Eng. Chem. Res. 47, 4029–4033. https://doi.org/10.1021/ie071573o.

Beamson, G., Briggs, D., 1993. High resolution XPS of organic polymers: the Scienta ESCA300 database. J. Chem. Educ. 70, A25. https://doi.org/10.1021/ed070pA25.5.

Bonifacio, A., Bonetti, L., Piantanida, E., De Nardo, L., 2023. Plasticizer design strategies enabling advanced applications of cellulose acetate. Eur. Polym. J. 197, 112360. https://doi.org/10.1016/j.eurpolymj.2023.112360.

Boulven, M., Quintard, G., Cottaz, A., Joly, C., Charlot, A., Fleury, E., 2019. Homogeneous acylation of cellulose diacetate: towards bioplastics with tuneable thermal and water transport properties. Carbohydr. Polym. 206, 674–684. https://doi.org/10.1016/j.carbpol.2018.11.030.

Bracciale, M.P., de Caprariis, B., Musivand, S., Damizia, M., De Filippis, P., 2024. Chemical recycling of cellulose acetate eyewear industry waste by hydrothermal treatment. Ind. Eng. Chem. Res. 63, 5078–5088. https://doi.org/10.1021/acs.iecr.3c04162.

Briggs, D., 2005. Surface Analysis of Polymers by XPS and Static SIMS. Cambridge University Press.

Cataldi, P., Bayer, I.S., Nanni, G., Athanassiou, A., Bonaccorso, F., Pellegrini, V., del Rio Castillo, A.E., Ricciardella, F., Artyukhin, S., Tronche, M.A., Gogotsi, Y., Cingolani, R., 2016. Effect of graphene nano-platelet morphology on the elastic modulus of soft and hard biopolymers. Carbon N.Y. 109, 331–339. https://doi.org/10.1016/j.carbon.2016.08.026.

Čespiva, J., Jadlovec, M., Výtisk, J., Serenčíšová, J., Ochodek, T., Honus, S., 2023. Softwood and solid recovered fuel gasification residual chars as sorbents for flue gas mercury capture. Environ. Technol. Innov. 29, 102970. https://doi.org/10.1016/j.eti.2022.102970.

Cherubini, F., Peters, G.P., Berntsen, T., Strømman, A.H., Hertwich, E., 2011. CO2 emissions from biomass combustion for bioenergy: atmospheric decay and

contribution to global warming. GCB Bioenergy 3, 413–426. https://doi.org/10.1111/j.1757-1707.2011.01102.x.
Cheshmak, A., Rezaee, B., Pakzad, H., Moosavi, A., Nouri-Borujerdi, A., 2025. Carbon-black based superhydrophobic coatings to achieve durable anti-condensation performance on cooled surfaces. Carbon n. y. 241, 120373. https://doi.org/10.1016/j.carbon.2025.120373.
Cho, W., Lee, S.H., Ju, W.S., Baek, Y., Lee, J.K., 2004. Conversion of natural gas to hydrogen and carbon black by plasma and application of plasma carbon black. Catal. Today 98, 633–638. https://doi.org/10.1016/j.cattod.2004.09.051.
Colazo, A.B., Sánchez, A., Font, X., Colón, J., 2015. Environmental impact of rejected materials generated in organic fraction of municipal solid waste anaerobic digestion plants: comparison of wet and dry process layout. Waste Manag. 43, 84–97. https://doi.org/10.1016/j.wasman.2015.06.028.
Czajka, K.M., 2021. The impact of the thermal lag on the interpretation of cellulose pyrolysis. Energy 121497. https://doi.org/10.1016/j.energy.2021.121497.
De la Rubia, M.A.A., Villamil, J.A.A., Rodriguez, J.J.J., Mohedano, A.F.F., 2018. Effect of inoculum source and initial concentration on the anaerobic digestion of the liquid fraction from hydrothermal carbonisation of sewage sludge. Renew. Energy 127, 697–704. https://doi.org/10.1016/j.renene.2018.05.002.
Elaigwu, S.E., Greenway, G.M., 2016. Chemical, structural and energy properties of hydrochars from microwave-assisted hydrothermal carbonization of glucose. Int. J. Ind. Chem. 7, 449–456. https://doi.org/10.1007/s40090-016-0081-0.
Fadipe, O.O., Oyewole, K.A., Adebanjo, A.U., Ajiferuke, A.T., Olukayode, O., 2025. Evaluating the reusability of carbon black recovered from waste tyres: an elemental and microstructural analysis. Results Surf. Interfaces 18, 100472. https://doi.org/10.1016/j.rsurfi.2025.100472.
Falco, C., Marco-Lozar, J.P., Salinas-Torres, D., Morallón, E., Cazorla-Amorós, D., Titirici, M.M., Lozano-Castelló, D., 2013. Tailoring the porosity of chemically activated hydrothermal carbons: Influence of the precursor and hydrothermal carbonization temperature. Carbon n. y. 62, 346–355. https://doi.org/10.1016/j.carbon.2013.06.017.
Fambri, L., Caria, R., Atzori, F., Ceccato, R., Lorenzi, D., 2020. Controlled Aging and Degradation of Selected Plastics in Marine Environment: 12 Months of Follow-up. pp. 89–100. DOI: 10.1007/978-3-030-45909-3_16.
Feng, S.Y., Li, S., Huang, W.Z., Niu, Q., Chen, D.Y., Fang, Z.M., Gao, L.J., Li, K., Lu, Q., 2024. Alkali pretreatment-assisted catalytic pyrolysis of waste cellulose acetate for selective preparation of levoglucosenone. J. Environ. Chem. Eng. 12, 113858. https://doi.org/10.1016/j.jece.2024.113858.
Ferrentino, R., Langone, M., Fiori, L., Andreottola, G., 2023. Full-scale sewage sludge reduction technologies: a review with a focus on energy consumption. Water 15, 615. https://doi.org/10.3390/w15040615.
Fu, D., Kurniawan, T.A., Gui, H., Li, H., Feng, S., Li, Q., Wang, Y., 2022. Role of Cu x O-anchored pyrolyzed hydrochars on H_2O_2-activated degradation of tetracycline: effects of pyrolysis temperature and pH. Ind. Eng. Chem. Res. 61, 8847–8857. https://doi.org/10.1021/acs.iecr.2c01100.
Gomes, M.M., Rabelo, C.A.B.S., Sakamoto, I.K., Silva, E.L., Varesche, M.B.A., 2021. Methane Production Using Brewery Spent Grain: Optimal Hydrothermolysis, Fermentation of Waste and Role of Microbial Populations. Waste and Biomass Valorization. DOI: 10.1007/s12649-021-01564-1.
Hämäläinen, A., Kokko, M., Tolvanen, H., Kinnunen, V., Rintala, J., 2024. Towards the implementation of hydrothermal carbonization for nutrients, carbon, and energy recovery in centralized biogas plant treating sewage sludge. Waste Manag. 173, 99–108. https://doi.org/10.1016/j.wasman.2023.11.012.
Hernandez-Charpak, Y.D., Mozrall, A.M., Williams, N.J., Trabold, T.A., Diaz, C.A., 2024. Biochar as a sustainable alternative to carbon black in agricultural mulch films. Environ. Res. 246, 117916. https://doi.org/10.1016/j.envres.2023.117916.
Howarth, R.W., 2021. Chapter 6: Methane and Climate Change, in: Environmental Impacts from Development of Unconventional Oil and Gas Reserves. pp. 1–21.
Howarth, R.W., Jacobson, M.Z., 2021. How green is blue hydrogen? Energy Sci. Eng. 9, 1676–1687. https://doi.org/10.1002/ese3.956.
Ischia, G., Cutillo, M., Guella, G., Bazzanella, N., Cazzanelli, M., Orlandi, M., Miotello, A., Fiori, L., 2022. Hydrothermal carbonization of glucose: Secondary char properties, reaction pathways, and kinetics. Chem. Eng. J. 449, 137827. https://doi.org/10.1016/j.cej.2022.137827.
Ischia, G., Goldfarb, J.L., Miotello, A., Fiori, L., 2023. Green solvents to enhance hydrochar quality and clarify effects of secondary char. Bioresour. Technol. 388, 129724. https://doi.org/10.1016/j.biortech.2023.129724.
Ischia, G., Marchelli, F., Bazzanella, N., Ceccato, R., Calvi, M., Guella, G., Gioia, C., Fiori, L., 2025. Cellulose acetates in hydrothermal carbonization: a green pathway to valorize residual bioplastics. ChemSusChem 18. https://doi.org/10.1002/cssc.202401163.
Jadlovec, M., Honus, S., Čespiva, J., 2024. Pyrolysis solid product as a sorbent for flue gases mercury capture — Part I: Sorbent formation and characteristics. Environ. Technol. Innov. 35, 103697. https://doi.org/10.1016/j.eti.2024.103697.
Jiang, H., Shao, J., Hu, Q., Zhu, Y., Cheng, W., Zhang, J., Fan, T., Yu, J., Yang, H., Zhang, X., Chen, H., 2024. Carbon black production characteristics and mechanisms from pyrolysis of rubbers. Fuel Process. Technol. 253, 108011. https://doi.org/10.1016/j.fuproc.2023.108011.
Jiang, H., Shao, J., Zhu, Y., Yu, J., Cheng, W., Yang, H., Zhang, X., Chen, H., 2023. Production mechanism of high-quality carbon black from high-temperature pyrolysis of waste tire. J. Hazard. Mater. 443, 130350. https://doi.org/10.1016/j.jhazmat.2022.130350.
Jianwen Xu, Wong, M., Wong, C.P., 2004. Super high dielectric constant carbon black-filled polymer composites as integral capacitor dielectrics, in: 2004 Proceedings. 54th Electronic Components and Technology Conference (IEEE Cat. No.04CH37546). IEEE, pp. 536–541. DOI: 10.1109/ECTC.2004.1319391.
Junga, R., Wzorek, M., Sobek, S., Sajdak, M., Yilmaz, E., 2024. Co-pyrolysis of animal manure and plastic waste study using TG-FTIR analysis. J. Anal. Appl. Pyrol. 181, 13–16. https://doi.org/10.1016/j.jaap.2024.106598.
Kelesidis, G.A., Benz, S., Pratsinis, S.E., 2023. Process design for carbon black size and morphology. Carbon n. y. 213, 118255. https://doi.org/10.1016/j.carbon.2023.118255.
Kelesidis, G.A., Crepaldi, P., Pratsinis, S.E., 2024. Oxidation dynamics of soot or carbon black accounting for its core-shell structure and pore network. Carbon n. y. 219, 118764. https://doi.org/10.1016/j.carbon.2023.118764.
Kiani, A., Sozio, N., Acocella, M.R., 2023. Sustainable functionalization of carbon black via dry ball milling. Mol. Syst. Des. Eng. 8, 942–949. https://doi.org/10.1039/d3me00042g.
Lombardi, L., Sahota, S., Polettini, A., Pomi, R., Rossi, A., Zonfa, T., Cema, G., Czerwińska, K., Magdziarz, A., Mikusińska, J., Śliz, M., Wilk, M., 2024. Valorization of cheese-making residues in biorefineries using different combinations of dark fermentation, hydrothermal carbonization and anaerobic digestion. Energy 305. https://doi.org/10.1016/j.energy.2024.132327.
Lombardi, L., Tuci, F., Śliz, M., Czerwińska, K., Fabrizi, S., Wilk, M., 2023. Life cycle assessment of the hydrothermal carbonization process applied to the wet fraction mechanically separated from municipal mixed waste. Waste Manag. 166, 181–193. https://doi.org/10.1016/j.wasman.2023.04.043.
Lucian, M., Volpe, M., Gao, L., Piro, G., Goldfarb, J.L., Fiori, L., 2018. Impact of hydrothermal carbonization conditions on the formation of hydrochars and secondary chars from the organic fraction of municipal solid waste. Fuel 233, 257–268. https://doi.org/10.1016/j.fuel.2018.06.060.
Luo, H., Wang, X., Krochmalny, K., Niedzwiecki, L., Czajka, K., Pawlak-Kruczek, H., Wu, X., Liu, X., Xiong, Q., 2022. Assessments and analysis of lumped and detailed pyrolysis kinetics for biomass torrefaction with particle-scale modeling. Biomass Bioenergy 166, 106619. https://doi.org/10.1016/j.biombioe.2022.106619.
Marchelli, F., Ferrentino, R., Ischia, G., Calvi, M., Andreottola, G., Fiori, L., 2023. Valorisation of eyewear bioplastics through Htc and anaerobic digestion: preliminary results. Detritus 23, 35–42. https://doi.org/10.31025/2611-4135/2023.18275.
Marchelli, F., Fiori, L., 2025. The growing problem of waste bioplastics disposal, and a way to tackle it. Waste Manag. 201, 114786. https://doi.org/10.1016/J.WASMAN.2025.114786.
Materazzi, M., Chari, S., Sebastiani, A., Lettieri, P., Paulillo, A., 2024. Waste-to-energy and waste-to-hydrogen with CCS: methodological assessment of pathways to carbon-negative waste treatment from an LCA perspective. Waste Manag. 173, 184–199. https://doi.org/10.1016/j.wasman.2023.11.020.
Melsom, J., 2003. Chapter 5 Testing Carbon Black, in: Basic Rubber Testing: Selecting Methods for a Rubber Test Program. ASTM International100 Barr Harbor Drive, PO Box C700, West Conshohocken, PA 19428-2959, pp. 89–104. DOI: 10.1520/MNL10435M.
Mikusińska, J., Szkadłubowicz, K., Prus, Z., Kuźnia, M., Gajek, M., Wilk, M., 2025. Fuel properties characterization of hydrochars derived from agricultural digestate. Renew. Energy 244. https://doi.org/10.1016/j.renene.2025.122639.
Mizeraczyk, J., Jasiński, M., 2016. Plasma processing methods for hydrogen production. EPJ Appl. Phys. 75, 1–7. https://doi.org/10.1051/epjap/2016150561.
Mlonka-Mędrala, A., Sieradzka, M., Magdziarz, A., 2022. Thermal upgrading of hydrochar from anaerobic digestion of municipal solid waste organic fraction. Fuel 324, 124435. https://doi.org/10.1016/j.fuel.2022.124435.
Musenich, L., Berardengo, M., Avalle, M., Haj-Ali, R., Sharabi, M., Libonati, F., 2024. Anisotropic mechanical and sensing properties of carbon black-polylactic acid nanocomposites produced by fused filament fabrication. Smart Mater. Struct. 33. https://doi.org/10.1088/1361-665X/ad6812.
Neffati, R., Brokken-Zijp, J.M.C., 2021. Structure and porosity of conductive carbon blacks. Mater. Chem. Phys. 260, 124177. https://doi.org/10.1016/j.matchemphys.2020.124177.
Okoye, C.O., Jones, I., Zhu, M., Zhang, Z., Zhang, D., 2021. Manufacturing of carbon black from spent tyre pyrolysis oil – a literature review. J. Clean. Prod. 279, 123336. https://doi.org/10.1016/j.jclepro.2020.123336.
Onyeka Okoye, C., Zhu, M., Jones, I., Zhang, J., Zhang, Z., Zhang, D., 2022. An investigation into the preparation of carbon black by partial oxidation of spent tyre pyrolysis oil. Waste Manag. 137, 110–120. https://doi.org/10.1016/j.wasman.2021.10.027.
Pantea, D., Darmstadt, H., Kaliaguine, S., Roy, C., 2003. Electrical conductivity of conductive carbon blacks: influence of surface chemistry and topology. Appl. Surf. Sci. 217, 181–193. https://doi.org/10.1016/S0169-4332(03)00550-6.
Pantea, D., Darmstadt, H., Kaliaguine, S., Sümmchen, L., Roy, C., 2001. Electrical conductivity of thermal carbon blacks: influence of surface chemistry. Carbon n. y. 39, 1147–1158. https://doi.org/10.1016/S0008-6223(00)00239-6.
Pfaff, G., 2022. Carbon black pigments. Phys. Sci. Rev. 7, 109–125. https://doi.org/10.1515/psr-2020-0152.
Piersa, P., Unyay, H., Szufa, S., Lewandowska, W., Modrzewski, R., Ślężak, R., Ledakowicz, S., 2022. An extensive review and comparison of modern biomass torrefaction reactors vs. biomass pyrolysis—Part 1. Energies 15, 2227. https://doi.org/10.3390/en15062227.
Qureshi, Z.A., Ali, H.M., Khushnood, S., 2018. Recent advances on thermal conductivity enhancement of phase change materials for energy storage system: a review. Int. J. Heat Mass Transf. 127, 838–856. https://doi.org/10.1016/j.ijheatmasstransfer.2018.08.049.
Rosenboom, J.-G., Langer, R., Traverso, G., 2022. Bioplastics for a circular economy. Nat. Rev. Mater. 7, 117–137. https://doi.org/10.1038/s41578-021-00407-8.

Rosner, F., Bhagde, T., Slaughter, D.S., Zorba, V., Stokes-Draut, J., 2024. Techno-economic and carbon dioxide emission assessment of carbon black production. J. Clean. Prod. 436, 140224. https://doi.org/10.1016/j.jclepro.2023.140224.
Rossi, F., De Bernardi, C., Frey, M., Niero, M., 2025. From past critiques to present challenges: a review of LCA approaches and results in the aluminum industry. Waste Manage. 204, 114900. https://doi.org/10.1016/j.wasman.2025.114900.
Rouxhet, P.G., Genet, M.J., 2011. XPS analysis of bio-organic systems. Surf. Interface Anal. 43, 1453–1470. https://doi.org/10.1002/sia.3831.
Schonvogel, D., Nowotny, M., Worieschеck, T., Multhaupt, H., Wagner, P., Dyck, A., Agert, C., Wark, M., 2019. Hydrothermal carbonization-derived carbon from waste biomass as renewable Pt support for fuel cell applications: role of carbon activation. Energy Technol. 7, 1–13. https://doi.org/10.1002/ente.201900344.
Seruga, P., Wilk, M., Cibis, E., Urbanowska, A., Niedźwiecki, Ł., 2025. The assessment of anaerobic digestion performance and efficiency in terms of waste collection. Energies 18, 4876. https://doi.org/10.3390/en18184876.
Sevilla, M., Fuertes, A.B., 2009a. Chemical and structural properties of carbonaceous products obtained by hydrothermal carbonization of saccharides. Chem. – A Eur J 15, 4195–4203. https://doi.org/10.1002/chem.200802097.
Sevilla, M., Fuertes, A.B., 2009b. The production of carbon materials by hydrothermal carbonization of cellulose. Carbon n. y. 47, 2281–2289. https://doi.org/10.1016/j.carbon.2009.04.026.
Shi, N., Liu, Q., He, X., Wang, G., Chen, N., Peng, J., Ma, L., 2019. Molecular structure and formation mechanism of hydrochar from hydrothermal carbonization of carbohydrates. Energy Fuels 33, 9904–9915. https://doi.org/10.1021/acs.energyfuels.9b02174.
Sieradzka, M., Rajca, P., Zajemska, M., Mlonka-Mędrala, A., Magdziarz, A., 2020. Prediction of gaseous products from refuse derived fuel pyrolysis using chemical modelling software - Ansys Chemkin-pro. J. Clean. Prod. 248. https://doi.org/10.1016/j.jclepro.2019.119277.
Slomkowski, S., Alemán, J.V., Gilbert, R.G., Hess, M., Horie, K., Jones, R.G., Kubisa, P., Meisel, I., Mormann, W., Penczek, S., Stepto, R.F.T., 2011. Terminology of polymers and polymerization processes in dispersed systems (IUPAC recommendations 2011). Pure Appl. Chem. 83, 2229–2259. https://doi.org/10.1351/PAC-REC-10-06-03.
Strzemiecka, B., Voelkel, A., Donate-Robles, J., Martín-Martínez, J.M., 2014. Assessment of the surface chemistry of carbon blacks by TGA-MS, XPS and inverse gas chromatography using statistical chemometric analysis. Appl. Surf. Sci. 316, 315–323. https://doi.org/10.1016/j.apsusc.2014.07.174.
Szufa, S., Unyay, H., Piersa, P., Kędzierska-Sar, A., Romanowska-Duda, Z., Likozar, B., 2025. Reduction of spruce phytotoxicity by superheated steam torrefaction and its use in stimulating the growth of ecological bio-products: Lemna minor L. Biomass Convers. Biorefinery. DOI: 10.1007/s13399-025-06508-6.
Taherian, R., 2018. Application of polymer-based composites: Bipolar plate of PEM fuel cells, Electrical Conductivity in Polymer-Based Composites: Experiments, Modelling, and Applications. Elsevier Inc. DOI: 10.1016/B978-0-12-812541-0.00007-0.
Thonglhueng, N., Sirisangsawang, R., Sukpancharoen, S., Phetyim, N., 2022. Optimization of iodine number of carbon black obtained from waste tire pyrolysis plant via response surface methodology. Heliyon 8, e11971. https://doi.org/10.1016/j.heliyon.2022.e11971.
Toth, P., Vikström, T., Molinder, R., Wiinikka, H., 2018. Structure of carbon black continuously produced from biomass pyrolysis oil. Green Chem. 20, 3981–3992. https://doi.org/10.1039/C8GC01539B.
Tran, H.N., Lee, C.-K., Nguyen, T.V., Chao, H.-P., 2018. Saccharide-derived microporous spherical biochar prepared from hydrothermal carbonization and different pyrolysis temperatures: synthesis, characterization, and application in water treatment. Environ. Technol. 39, 2747–2760. https://doi.org/10.1080/09593330.2017.1365941.
Ubene, M., MacDermid-Watts, K., Dutta, A., van der Kuur, C., 2024. High surface area microporous activated carbon from corn fiber using graphene oxide-assisted hydrothermal carbonization. ACS Sustain. Resour. Manag. 1, 1053–1067. https://doi.org/10.1021/acssusresmgt.3c00025.
Wagner, A.D., Naumkin, A.V., Kraut-Vass, A., Allison, J.W., Powell, C.J., Rumble, J.R.J., 2003. NIST Standard Reference Database 2.0.
Wang, R., Jia, J., Jin, Q., Chen, H., Liu, H., Yin, Q., Zhao, Z., 2022. Forming mechanism of coke microparticles from polymerization of aqueous organics during hydrothermal carbonization process of biomass. Carbon n. y. 192, 50–60. https://doi.org/10.1016/j.carbon.2022.02.030.
Wang, S., Mandfloen, P., Jönsson, P., Yang, W., 2021. Synergistic effects in the copyrolysis of municipal sewage sludge digestate and salix: Reaction mechanism, product characterization and char stability. Appl. Energy 289, 116687. https://doi.org/10.1016/j.apenergy.2021.116687.
Wang, X., Huang, B., Wang, Y., Liu, J., Long, Y., Daigo, I., 2023. The impact of allocation methods on carbon benefits - a case study of construction waste recycling. Resour. Conserv. Recycl. 199, 107269. https://doi.org/10.1016/j.resconrec.2023.107269.
Wang, Y., Hu, Y.J., Hao, X., Peng, P., Shi, J.Y., Peng, F., Sun, R.C., 2020. Hydrothermal synthesis and applications of advanced carbonaceous materials from biomass: a review. Adv. Compos. Hybrid Mater. 3, 267–284. https://doi.org/10.1007/s42114-020-00158-0.
Wen, Y., Bella, Song, G., Chang, J., Kawi, S., Wang, C.-H., 2025. Machine learning insights into the production and characteristics of carbon nanotubes from methane catalytic decomposition. J. Energy Chem. 104, 726–739. DOI: 10.1016/j.jechem.2025.01.023.
Wen, Y., Shi, Z., Wang, S., Mu, W., Jönsson, P.G., Yang, W., 2021. Pyrolysis of raw and anaerobically digested organic fractions of municipal solid waste: Kinetics, thermodynamics, and product characterization. Chem. Eng. J. 415, 129064. https://doi.org/10.1016/j.cej.2021.129064.
Wennebro, J., Vikström, T., Reinsdorf, O., Wiinikka, H., 2025. Influence of feedstock water content on renewable carbon black production through high-temperature pyrolysis of upgraded bio-oils. Energy Fuels 39, 7805–7814. https://doi.org/10.1021/acs.energyfuels.5c00308.
Wilk, M., Magdziarz, A., Kalemba-Rec, I., Szymańska-Chargot, M., 2020. Upgrading of green waste into carbon-rich solid biofuel by hydrothermal carbonization: the effect of process parameters on hydrochar derived from acacia. Energy 202, 117717. https://doi.org/10.1016/j.energy.2020.117717.
Williams, J.H., Gbadomosi, M., Greytak, A.B., Myrick, M.L., 2023. Measuring the surface area of carbon black using BET isotherms: an experiment in physical chemistry. J. Chem. Educ. 100, 4838–4844. https://doi.org/10.1021/acs.jchemed.3c00764.
Wnukowski, M., 2023. Methane pyrolysis with the use of plasma: review of plasma reactors and process products. Energies 16. https://doi.org/10.3390/en16186441.
Wortmann, M., Keil, W., Brockhagen, B., Biedinger, J., Westphal, M., Weinberger, C., Diestelhorst, E., Hachmann, W., Zhao, Y., Tiemann, M., Reiss, G., Hüsgen, B., Schmidt, C., Sattler, K., Frese, N., 2022. Pyrolysis of sucrose-derived hydrochar. J. Anal. Appl. Pyrol. 161, 105404. https://doi.org/10.1016/j.jaap.2021.105404.
Wortmann, M., Keil, W., Diestelhorst, E., Westphal, M., Haverkamp, R., Brockhagen, B., Biedinger, J., Bondzio, L., Weinberger, C., Baier, D., Tiemann, M., Hütten, A., Hellweg, T., Reiss, G., Schmidt, C., Sattler, K., Frese, N., 2023. Hard carbon microspheres with bimodal size distribution and hierarchical porosity via hydrothermal carbonization of trehalose. RSC Adv. 13, 14181–14189. https://doi.org/10.1039/D3RA01301D.
Wu, S., Wang, Z., Guo, S., Cai, Y., Zhang, J., Huangfu, C., Huang, Y., Ma, L., Zhao, W., 2024. Life-cycle-based reconfiguration of sustainable carbon black production: Integrated conventional technique with waste tire pyrolysis and its future improvement potentials. J. Clean. Prod. 442, 141022. https://doi.org/10.1016/j.jclepro.2024.141022.
Yan, Q., Li, R., 2015. Synthesis and Characterization of carbon nanospheres obtained by hydrothermal carbonization of wood-derived and other saccharides. Trends Renew. Energy 1, 119–128. https://doi.org/10.17737/tre.2015.1.2.0012.
Yu, L., Falco, C., Weber, J., White, R.J., Howe, J.Y., Titirici, M.M., 2012. Carbohydrate-derived hydrothermal carbons: a thorough characterization study. Langmuir 28, 12373–12383. https://doi.org/10.1021/la3024277.